Journal of Computational Physics 469 (2022) 111549

Contents lists available at ScienceDirect

Journal of Computational Physics

www.elsevier.com/locate/jcp

Short note

Analytic continuation from limited noisy Matsubara data

Lexing Ying [1]

Department of Mathematics, Stanford University, Stanford, CA 94305, United States of America

ARTICLE INFO

Article history:
Received 12 March 2022
Received in revised form 13 July 2022
Accepted 15 August 2022
Available online 24 August 2022

Keywords:
Rational approximation
Prony's method
Analytic continuation

ABSTRACT

This note proposes new algorithms for estimating spectral distribution from limited noisy Matsubara data. We consider both the cases of the spectral distribution with a sparse or a continuous support. In both cases, the proposed algorithm first constructs an accurate approximation of the Matsubara data, uses a novel conformal map to transform the domain, and applies Prony's method to estimate the spectral distribution. Numerical results are provided to demonstrate the performance of the algorithms.

1. Introduction

For a real non-negative spectral distribution $A(x)$ defined on $\mathbb{R}$, the Green's function $G(z)$ for $z \in \mathbb{C}$ associated with $A(x)$ is defined as

$$G(z) = \int_{\mathbb{R}} \frac{1}{z-x} A(x) \mathrm{d}x.$$

In this note, we are interested in the analytic continuation problem of recovering $A(x)$ from $G(z)$. This is known to be an ill-posed inverse problem [26].

In many-body quantum mechanics, for a fixed inverse temperature β, the fermionic Matsubara grid is defined as $\{z_n = \frac{(2n+1)\pi}{\beta} i\}_{n\in\mathbb{Z}}$. A particular important instance of the analytic continuation problem is to estimate $A(x)$ from potentially noisy values of $G(z_n)$ at a finite Matsubara grid $z_{-N}, \ldots, z_{N-1}$ for some integer N.

In most quantum mechanics computations, we are faced with two typical cases.

- The sparse case, where the support of $A(x)$ consists of a small number of points in $\mathbb{R}$. This is often the situation when one works with a small molecular system.
- The continuous case, where $A(x)$ is a positive continuous function over $\mathbb{R}$. This case often appears when working with a large condensed matter system.

1.1. Related work

In computational physics and chemistry, the Matsubara Green's function data can be obtained from finite temperature simulations using for example GW theory or quantum Monte Carlo. The spectral function $A(x)$ describes the single-particle

E-mail address: lexing@stanford.edu.

[1] The work of L.Y. is partially supported by National Science Foundation under award DMS-2011699.

https://doi.org/10.1016/j.jcp.2022.111549
0021-9991/

excitation spectrum [7]. Many methods have been proposed for this analytic continuation problem, including Pade approximation [2,25,28], maximum entropy methods [1,15,16,18,23], stochastic analytic continuation [12,17,24,27], and the more recent development based on Nevanlinna functions [9,10].

This problem is also highly related to several other well-studied problems, including rational function approximation and interpolation [3,4,6,11,14,20,29], approximation with exponential sums [5,21], and hybridization fitting [19].

1.2. Contributions

This note proposes new algorithms for both the sparse and the continuous support cases. Since the problem is ill-conditioned, some regularization or prior information is needed for the problem to be well-posed.

In the sparse support case, the fact that $A(x)$ is a supported at a sum number of real points provides a strong prior. The actual implementation depends on whether the support of $A(x)$ is well-separated from origin. By well-separated, we mean that the support of $A(x)$ does not overlap with an interval $[-\epsilon, \epsilon]$ where ϵ is larger than or at least comparable to π/β.

- If the support of $A(x)$ is well-separated from the origin, $G(z)$ is analytic in the strip $[-\epsilon, \epsilon] \times [-\frac{(2N-1)\pi}{\beta} i, \frac{(2N-1)\pi}{\beta} i]$ in the complex plane. The proposed algorithm proceeds by (1) constructing an analytic approximation of $G(z)$ over $[-\frac{(2N-1)\pi}{\beta} i, \frac{(2N-1)\pi}{\beta} i]$, (2) using a conformal map to unzip this interval into a unit circle, (3) applying Prony's method to identify the poles in the transformed domain, and (4) finally recovering pole locations the original domain and computing the weights.
- If the support of $A(x)$ is not well-separated from the origin, the algorithm replaces the first step by constructing instead an analytic approximation of $G(z)$ over $(-\infty, -\frac{\pi i}{\beta}] \cup [\frac{\pi i}{\beta}, \infty)$ (an arc on the Riemann sphere) and the second step by unzipping this arc. The remaining steps are similar.

In the continuous support case, $G(z)$ is only analytic in the upper half plane. Motivated by the concept of scattering resonances [8], one physically meaningful prior is that the Green function $G(z)$ associated with $A(x)$ can be well approximated by a Green function induced by a small number of *pseudo poles* located in the lower half plane. Under this prior, the algorithm proceeds by (1) constructing an accurate approximation of $G(z)$ over the interval $[\frac{\pi}{\beta} i, \frac{(2N-1)\pi}{\beta} i]$ of the positive imaginary axis, (2) using a conformal map to unzip this interval into a disk, (3) applying Prony's method to identify the poles in the transformed domain, and (4) identifying the pseudo poles in the lower half plane plus evaluating the spectral function $A(x)$.

The rest of the note is organized as follows. Section 2 describes the algorithm for the sparse support case and presents some numerical results. Section 3 is concerned with the continuous support case.

2. Sparse support

In the sparse support case, $A(x)$ takes the form

$$A(x) = \sum_j A_j \delta_{\xi_j}(x),$$

where $\{\xi_j\}$ are the pole locations on the real axis and $\{A_j\}$ are the weights. $G(z)$ can then be written as

$$G(z) = \sum_j \frac{1}{z - \xi_j} A_j.$$

The actual algorithm depends on whether $A(x)$ is supported near the origin. When the support of $A(x)$ is well-separated from the origin, we refer to it the gapped case. When the support of $A(x)$ is close to or even overlaps with the origin, we refer to it as the gapless case.

2.1. Gapped case

In the gapped case, the support of $A(x)$ is assumed to be bounded away from the interval $[-\epsilon, \epsilon]$, where ϵ is larger than or at least comparable to β/π. Due to this gap, $G(z)$ is analytic in the strip $[-\epsilon, \epsilon] \times [-\frac{(2N-1)\pi}{\beta} i, \frac{(2N-1)\pi}{\beta} i]$.

Step 1. We first construct an analytic approximation of $G(z)$ for $z \in [-\frac{(2N-1)\pi}{\beta} i, \frac{(2N-1)\pi}{\beta} i]$. The approximation adopted here is of the form

$$G(z) \approx \sum_k \frac{1}{z - x_k} X_k,$$

where $\{x_k\}$ is a set of real locations in $(-\infty, -\epsilon] \bigcup [\epsilon, \infty)$. To motivate the choice of $\{x_k\}$, instead of viewing $(-\infty, -\epsilon] \bigcup [\epsilon, \infty)$ as the union of two semi-infinite intervals, we can consider the Riemann sphere and regard it as

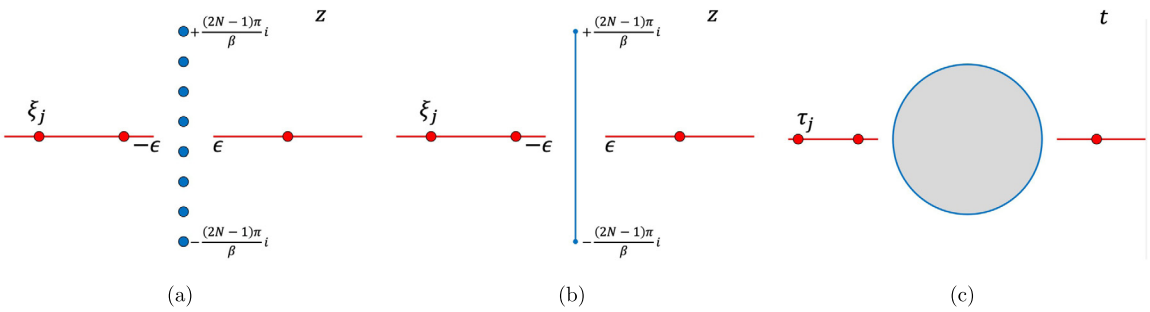

Fig. 1. Sparse support, gapped case. (a) Problem configuration where the blue dots are the fermionic Matsubara grid and the red dots are the unknown support of $A(x)$. (b) $\tilde{G}(z)$ approximates $G(z)$ over $[-\frac{(2N-1)\pi}{\beta}i, \frac{(2N-1)\pi}{\beta}i]$ and allows for random access. (c) Use a conformal map to unzip the interval $[-\frac{(2N-1)\pi}{\beta}i, \frac{(2N-1)\pi}{\beta}i]$ into a unit disk. The mapped poles are denoted as $\{\tau_j\}$.

an arc passing the point of infinity. In order to place an approximation grid on this arc, it is convenient to map it first to a finite interval. To achieve this, we use the conformal map

$$z \leftrightarrow \epsilon/z: \quad (-\infty, -\epsilon] \bigcup [\epsilon, \infty) \leftrightarrow [-1, 1].$$

For a finite interval, it is well-known that the Chebyshev grid is a good choice for approximation and interpolation. Therefore, we first pick the Chebyshev grid $\left\{\cos\left(\frac{k\pi}{N_x-1}\right)\right\}_{0\le k<N_x}$ of $[-1, 1]$ with N_x equal to a constant multiple of N. This grid is then mapped back with $z \leftrightarrow \epsilon/z$ to obtain

$$x_k = \frac{\epsilon}{\cos\left(\frac{k\pi}{N_x-1}\right)}.$$

Given $\{x_k\}_{0\le k<N_x}$, we solve for the real positive weights $\{X_k\}_{0\le k<N_x}$ from the constrained least-squares problem

$$\min_{X_k>0} \sum_{-N\le n<N} \left| G(z_n) - \sum_{0\le k<N_x} \frac{1}{z_n - x_k} X_k \right|^2. \tag{1}$$

With $\{x_k\}_{0\le k<N_x}$ and $\{X_k\}_{0\le k<N_x}$ available, the function

$$\tilde{G}(z) \equiv \sum_{0\le k<N_x} \frac{1}{z - x_k} X_k \tag{2}$$

is an accurate approximation to $G(z)$ over $[-\frac{(2N-1)\pi}{\beta}i, \frac{(2N-1)\pi}{\beta}i]$ that allows for random access (see Fig. 1(b)).

Step 2. Introduce the following conformal map

$$z(t) = \frac{(2N-1)\pi}{\beta} \cdot \frac{t - t^{-1}}{2} \tag{3}$$

that unzips the interval $[-\frac{(2N-1)\pi}{\beta}i, \frac{(2N-1)\pi}{\beta}i]$ in the z plane to the unit disk $\mathbb{D}$ in the t plane (see Fig. 1(c)).

In the t plane, the push-forward $G(t) \equiv G(z(t))$ of $G(z)$ is analytic outside $\mathbb{D}$ except at the images of $\{\xi_j\}$. Therefore, it takes the form

$$G(t) = \sum_j \frac{T_j}{t - \tau_j} + \text{analytic},$$

where $\{\tau_j\}$ are the images of $\{\xi_j\}$ and $\{T_j\}$ are the new weights. In addition, the push-forward $\tilde{G}(t) \equiv \tilde{G}(z(t))$ of $\tilde{G}(z)$ is an approximation of $G(t)$ over the unit circle that allows for random access.

A key observation is that if one can identify the poles $\{\tau_j\}$ in the t plane, we can map them back to the z plane to obtain the poles $\{\xi_j\}$ of $G(z)$.

Step 3. In order to find $\{\tau_j\}$, consider the integrals

$$\frac{1}{2\pi i} \int_\gamma \frac{G(t)}{t^k} \frac{\mathrm{d}t}{t} \tag{4}$$

with $k \ge 1$, where the contour γ is the unit circle in the t plane in the counterclockwise orientation. For any $k \ge 1$,

$$\frac{1}{2\pi i}\int_{\gamma}\frac{G(t)}{t^k}\frac{\mathrm{d}t}{t}=-\sum_j\frac{1}{2\pi i}\int_{\gamma_j}\frac{G(t)}{t^k}\frac{\mathrm{d}t}{t}=-\sum_j T_j\tau_j^{-(k+1)}, \tag{5}$$

where each γ_j is an infinitesimal circle around the pole τ_j. Here, the first equality comes from the facts that $G(t)/t^{k+1}$ is analytic in the region outside γ and $\{\gamma_j\}$ and that $G(t)/t^{k+1}$ decays rapidly at infinity. The second equality holds because the residue of $G(t)/t^{k+1}$ at τ_j is $T_j\tau_j^{-(k+1)}$. This shows that the integrals (4) for $k\geq 1$ contain information about the poles $\{\tau_j\}$.

Since the integral (4) is over the unit circle, it is closely related to the Fourier transform of $G(e^{i\theta})$, the restriction of $G(t)$ to the unit circle

$$\frac{1}{2\pi i}\int_{\gamma}\frac{G(t)}{t^k}\frac{\mathrm{d}t}{t}=\frac{1}{2\pi i}\int_0^{2\pi}G(e^{i\theta})e^{-ik\theta}i\mathrm{d}\theta=\frac{1}{2\pi}\int_0^{2\pi}G(e^{i\theta})e^{-ik\theta}\mathrm{d}\theta\equiv\hat{G}_k. \tag{6}$$

As we can approximate $G(t)$ along the unit circle with $\tilde{G}(t)$, $\hat{G}_k$ can be approximated. Putting (5) and (6) together, we have for $k\geq 1$

$$\hat{G}_k=\frac{1}{2\pi i}\int_{\gamma}\frac{G(t)}{t^k}\frac{\mathrm{d}t}{t}=-\sum_j T_j\tau_j^{-(k+1)}. \tag{7}$$

To recover $\{\tau_j\}$ outside $\mathbb{D}$, we apply Prony's method [22] to these Fourier coefficients of the positive frequencies. Following [30], define the semi-infinite vector

$$\hat{G}_+\equiv\begin{bmatrix}\hat{G}_1\\ \hat{G}_2\\ \vdots\end{bmatrix}\equiv\frac{1}{2\pi i}\int_{\gamma}G(t)\begin{bmatrix}t^{-2}\\ t^{-3}\\ \vdots\end{bmatrix}\mathrm{d}t\equiv\begin{bmatrix}-\sum_j T_j\tau_j^{-2}\\ -\sum_j T_j\tau_j^{-3}\\ \vdots\end{bmatrix},$$

where these identities follow from (7). Let S be the operator that shifts the semi-infinite vector upward (and drops the first element). For any τ_j

$$S\begin{bmatrix}\tau_j^{-2}\\ \tau_j^{-3}\\ \vdots\end{bmatrix}=\begin{bmatrix}\tau_j^{-3}\\ \tau_j^{-4}\\ \vdots\end{bmatrix},\quad\text{i.e.,}\quad(S-\tau_j^{-1})\begin{bmatrix}\tau_j^{-2}\\ \tau_j^{-3}\\ \vdots\end{bmatrix}=0.$$

Since the operators $S-\tau_j^{-1}$ commute with each other,

$$\prod_{\ell}(S-\tau_\ell^{-1})\begin{bmatrix}\tau_j^{-2}\\ \tau_j^{-3}\\ \vdots\end{bmatrix}=0. \tag{8}$$

Since the product $\prod_\ell(S-\tau_\ell^{-1})$ is independent of any specific j and $\hat{G}_+$ is a linear combination of these semi-infinite vectors with weights $-T_j$, we hold

$$\prod_{\ell}(S-\tau_\ell^{-1})\hat{G}_+=0. \tag{9}$$

Let us introduce the polynomial

$$\prod_{\ell}(t-\tau_\ell^{-1})\equiv p(t)\equiv p_0t^0+\cdots+p_dt^d,$$

where the degree d is equal to the number of poles outside $\mathbb{D}$. Then (9) becomes

$$p(S)\hat{G}_+\equiv p_0(S^0\hat{G}_+)+\cdots+p_d(S^d\hat{G}_+)=0,\quad\text{i.e.,}\quad\begin{bmatrix}\hat{G}_1 & \hat{G}_2 & \cdots & \hat{G}_{d+1}\\ \hat{G}_2 & \hat{G}_3 & \cdots & \hat{G}_{d+2}\\ \vdots & \vdots & \ddots & \vdots\end{bmatrix}\begin{bmatrix}p_0\\ \dots\\ p_d\end{bmatrix}=0. \tag{10}$$

This implies that the number of poles $\{\tau_j\}$ is equal to the smallest value d such that the matrix in (10) is rank deficient. $[p_0,\dots,p_d]^{\mathsf{T}}$ can be computed as a non-zero vector in the null-space of this matrix and the roots of $p(t)\equiv p_0t^0+\dots+p_dt^d$ are $\{\tau_j^{-1}\}$. Taking inverse of these roots gives the poles $\{\tau_j\}$.

Step 4. Applying the map (3) to $\{\tau_j\}$ leads to the poles $\{\xi_j\}$, i.e., the support of $A(x)$ in the z plane. With $\{\xi_j\}$ identified, we solve the constrained convex optimization problem

$$\min_{A_j \geq 0} \sum_{-N \leq n < N} \left| G(z_n) - \sum_j \frac{A_j}{z_n - \xi_j} \right|^2 \tag{11}$$

for the weights $\{A_j\}$.

Implementation details. To implement this algorithm, we need to address several numerical issues.

- The computation of the weights $\{X_k\}$ in (1) is solved with CVX [13].
- The semi-infinite matrix in (10). In the implementation, pick a value $d_{\max}$ that is believed to be the upper bound of the number of poles and form the matrix

$$H = \begin{bmatrix} \hat{G}_1 & \hat{G}_2 & \cdots & \hat{G}_{d_{\max}} \\ \hat{G}_2 & \hat{G}_3 & \cdots & \hat{G}_{(d_{\max}+1)} \\ \vdots & \vdots & \ddots & \vdots \\ \hat{G}_l & \hat{G}_{l+1} & \cdots & \hat{G}_{(d_{\max}+l-1)} \end{bmatrix} \tag{12}$$

  with $l \geq d_{\max}$. In practice, $l = d_{\max}$ is enough.
- The numerical estimation of the rank d in (10). Let $s_1, s_2, \ldots, s_{d_{\max}}$ be the singular values of the matrix H. The numerical rank d is set to be the index with the largest singular value drop in the logarithmic scale (before reaching the noise level).
- The computation of the vector $[p_0, \ldots, p_d]^{\mathsf{T}}$. We first compute the singular value decomposition (SVD) of

$$\begin{bmatrix} \hat{G}_1 & \hat{G}_2 & \cdots & \hat{G}_{d+1} \\ \hat{G}_2 & \hat{G}_3 & \cdots & \hat{G}_{d+2} \\ \vdots & \vdots & \ddots & \vdots \\ \hat{G}_l & \hat{G}_{l+1} & \cdots & \hat{G}_{d+l} \end{bmatrix},$$

  a submatrix of (12). $[p_0, \ldots, p_d]^{\mathsf{T}}$ is then chosen to be the last column of the V matrix of the SVD.
- The matrix H in (12) requires the Fourier coefficients $\hat{G}_k$ for $k = 1, \ldots, (d_{\max} + l - 1)$. Since the push-forward $\tilde{G}(t)$ of $\tilde{G}(z)$ is an approximation of $G(t)$ over the unit circle, we have

$$\hat{G}_k \approx \frac{1}{2\pi} \int_0^{2\pi} \tilde{G}(e^{i\theta}) e^{-ik\theta} \mathrm{d}\theta.$$

  To approximate this integral, define $\theta_n = \frac{2\pi n}{N_\theta}$ for $n = 0, \ldots, N_\theta - 1$, where N_θ is chosen to be a constant multiple of N. With the trapezoidal quadrature rule,

$$\hat{G}_k \approx \frac{1}{N_\theta} \sum_{n=0}^{N_\theta - 1} \tilde{G}(e^{i\theta_n}) e^{-ik\theta_n}.$$

  The trapezoidal rule is exponentially convergent for smooth functions when the step size $\frac{2\pi}{N_\theta}$ is sufficient small. In the current setting, this corresponds to $N_\theta \gg \frac{(2N-1)\pi/\beta}{\epsilon}$. Our choice of N_θ satisfies this condition because ϵ is larger than π/β. Therefore, the error due to the numerical quadrature is exponentially small and does not affect the accuracy of $\hat{G}_k$.
- The constrained optimization problem (11) is solved with CVX [13].

Numerical results. The inverse temperature is $\beta = 100$ and the number of Matsubara points is $N = 128$. For fixed values of β and N, the smaller the gap the harder the problem.

The noise model in $G(z_n)$ is additive

$$G(z_n) \leftarrow G(z_n) + \sigma \cdot M \cdot N_{\mathbb{C}}(0, 1), \tag{13}$$

where $M = \left(\sum_n |G(z_n)|^2 / N\right)^{1/2}$ is the average magnitude and $N_{\mathbb{C}}(0, 1)$ is the standard complex normal distribution. The noise levels in the experiments are $\sigma = 10^{-4}$, 10^{-3}, and 10^{-2}.

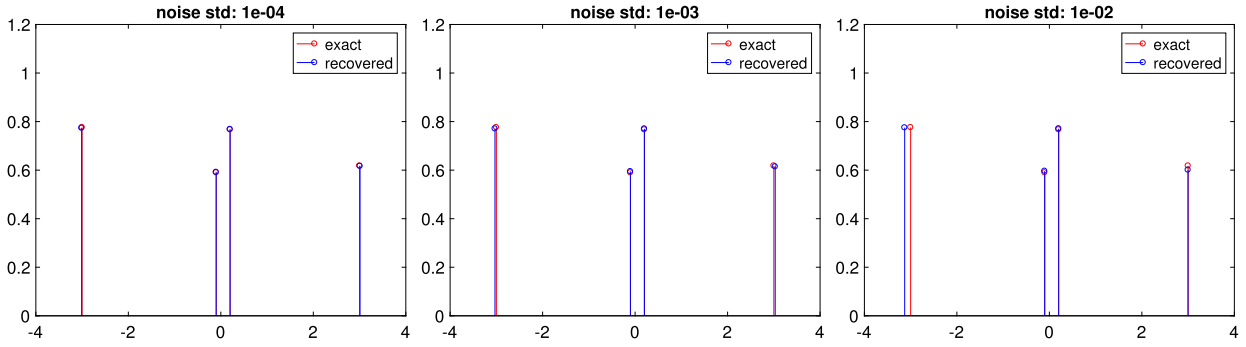

Fig. 2. Sparse support and gapped case. Results with gap $\epsilon = 0.1$ at different noise levels.

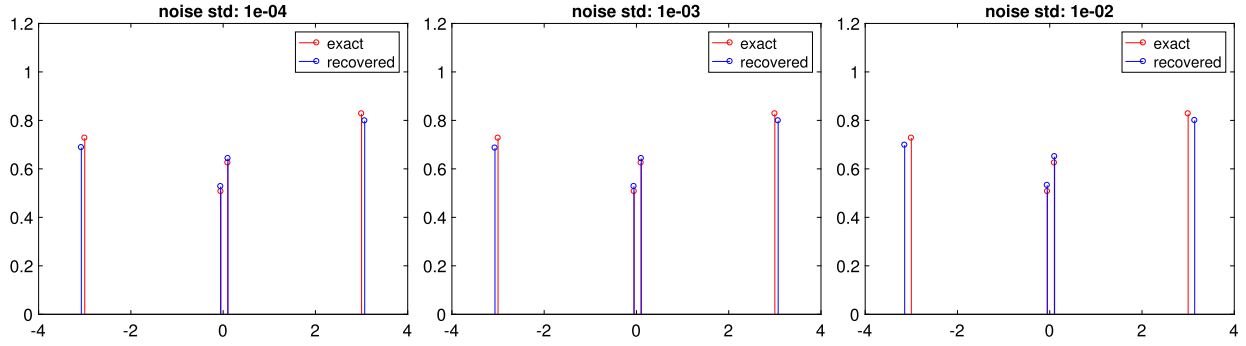

Fig. 3. Sparse support and gapped case. Results with gap $\epsilon = 0.05$ at different noise levels.

In the first example, the gap is $\epsilon = 0.1$ and the results are summarized in Fig. 2. For $\sigma = 10^{-4}$, the algorithm results in an accurate reconstruction in terms of both the pole locations and the weights. At $\sigma = 10^{-3}$, the reconstruction is still quite accurate. At $\sigma = 10^{-2}$, there are noticeable errors in the pole locations, while the weights are still quite accurate.

In the second example, the gap is $\epsilon = 0.05$ and the results are presented in Fig. 3. The numerical behaviors are similar to the $\epsilon = 0.1$ case, though the errors are larger due to the smaller gap ϵ.

2.2. Gapless case

When the support of $A(x)$ contains the origin, $G(z)$ fails to be analytic there. Even when the support of $A(x)$ is only close to the origin, $G(z)$ can become too oscillatory for accurate numerical approximations. Therefore, instead of approximating $G(z)$ over the interval $[-\frac{(2N-1)\pi}{\beta}i, \frac{(2N-1)\pi}{\beta}i]$, we consider approximating $G(z)$ over $z \in (-\infty, -\frac{\pi i}{\beta}] \cup [\frac{\pi i}{\beta}, \infty)$. This is in fact an arc on the Riemman sphere and $G(z)$ is analytic in a neighborhood of it.

Step 1. We first construct an analytic approximation of $G(z)$ over $(-\infty, -\frac{\pi i}{\beta}] \cup [\frac{\pi i}{\beta}, \infty)$. The approximation is again of the form $G(z) \approx \sum_k \frac{1}{z - x_k} X_k$, where $\{x_k\}$ is a set of points on the real axis. To motivate the choice of $\{x_k\}$, consider the conformal map

$$w = \frac{z - q}{z + q}, \quad z = -q \cdot \frac{w + 1}{w - 1},$$

where $q = \frac{\sqrt{2N-1}\pi}{\beta}i$. This map makes the upper half plane in z to the unit disk in w, the real axis in z to the unit circle in w, and the point q in z to the origin in w. Motivated by the trapezoidal quadrature rule, we choose an equally spaced grid of size N_x on the unit circle in w with N_x equal to a constant multiple of N. This grid is then mapped back to the z plane to give $\{x_k\}_{0 \le k < N_x}$.

Given $\{x_k\}_{0 \le k < N_x}$, we solve for the real positive weights $\{X_k\}$ from the constrained least-squares problem

$$\min_{X_k > 0} \sum_n \left| G(z_n) - \sum_k \frac{1}{z_n - x_k} X_k \right|^2.$$

With $\{x_k\}$ and $\{X_k\}$ available now, the function

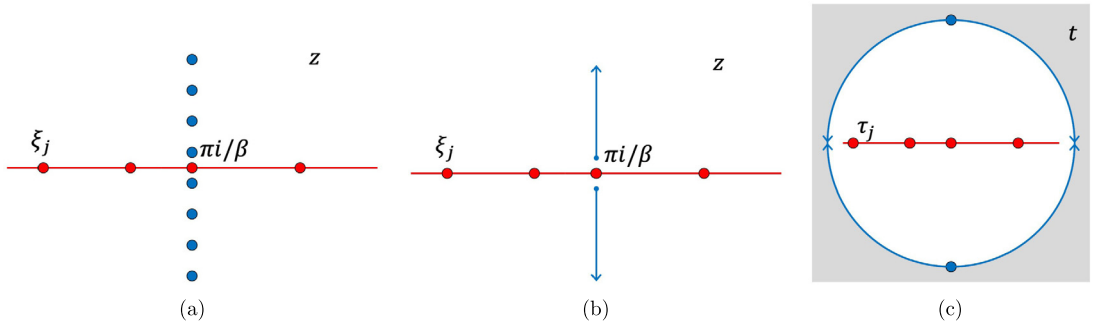

Fig. 4. Sparse support, gapless case. (a) Problem configuration where the blue dots are the fermionic Matsubara grid and the red dots are the unknown support of $A(x)$. (b) $\tilde{G}(z)$ approximates $G(z)$ over $(-\infty, -\frac{\pi i}{\beta}] \cup [\frac{\pi i}{\beta}, \infty)$ and allows for random access. (c) Use a conformal map to unzip $(-\infty, -\frac{\pi i}{\beta}] \cup [\frac{\pi i}{\beta}, \infty)$ into a unit disk. The mapped poles are denoted as $\{\tau_j\}$.

$$\tilde{G}(z) \equiv \sum_k \frac{1}{z - x_k} X_k$$

serves as an accurate approximation to $G(z)$ over $(-\infty, -\frac{\pi i}{\beta}] \cup [\frac{\pi i}{\beta}, \infty)$ that allows for random access (see Fig. 4(b)).

Step 2. Introduce the conformal map

$$z = -\frac{\pi}{\beta} \cdot \frac{2}{t - t^{-1}}, \tag{14}$$

that unzips $(-\infty, -\frac{\pi i}{\beta}] \cup [\frac{\pi i}{\beta}, \infty)$ in the z plane to the unit disk $\mathbb{D}$ in the t plane (see Fig. 4(c)). The z plane is mapped into the interior of the unit disk.

In the t plane, the push-forward $G(t) \equiv G(z(t))$ of $G(z)$ is analytic inside $\mathbb{D}$ except at the images of $\{\xi_j\}$. Therefore, it takes the form

$$G(t) = \sum_j \frac{T_j}{t - \tau_j} + \text{analytic},$$

where the poles $\{\tau_j\}$ are the images of $\{\xi_j\}$. The push-forward $\tilde{G}(t) \equiv \tilde{G}(z(t))$ of $\tilde{G}(z)$ is an approximation of $G(t)$ over the unit circle that allows for random access. If one can identify the poles $\{\tau_j\}$ in the t plane, we can map them back to the z plane to obtain the poles $\{\xi_j\}$ of $G(z)$.

Step 3. To find $\{\tau_j\}$, consider the integrals

$$\frac{1}{2\pi i} \int_\gamma \frac{G(t)}{t^k} \frac{\mathrm{d}t}{t}$$

with $k \le -1$ instead, where the contour γ is again the unit circle in the counterclockwise orientation. For any $k \le -1$,

$$\frac{1}{2\pi i} \int_\gamma \frac{G(t)}{t^k} \frac{\mathrm{d}t}{t} = \sum_j \frac{1}{2\pi i} \int_{\gamma_j} \frac{G(t)}{t^k} \frac{\mathrm{d}t}{t} = \sum_j T_j \tau_j^{-(k+1)},$$

where each γ_j is an infinitesimal circle around the pole τ_j. Here, the first equality comes from the facts that $G(t)/t^{k+1}$ is analytic inside γ but outside $\{\gamma_j\}$. The second equality holds because the residue of $G(t)/t^{k+1}$ at τ_j is $T_j \tau_j^{-(k+1)}$. This demonstrates that the integrals for $k \le -1$ contain information about the poles $\{\tau_j\}$.

Since the integral is over the unit circle, it is equal to the Fourier coefficients of negative frequencies. In summary, we have for $k \le -1$

$$\hat{G}_k = \frac{1}{2\pi i} \int_\gamma \frac{G(t)}{t^k} \frac{\mathrm{d}t}{t} = \sum_j T_j \tau_j^{-(k+1)}.$$

To recover the poles $\{\tau_j\}$ inside $\mathbb{D}$, we apply Prony's method to these Fourier coefficients of the negative frequencies. Define the semi-infinite vector

$$\hat{G}_- \equiv \begin{bmatrix} \hat{G}_{-1} \\ \hat{G}_{-2} \\ \vdots \end{bmatrix} \equiv \frac{1}{2\pi i} \int_\gamma G(t) \begin{bmatrix} t^0 \\ t^1 \\ \vdots \end{bmatrix} \mathrm{d}t \equiv \begin{bmatrix} \sum_j T_j \tau_j^0 \\ \sum_j T_j \tau_j^1 \\ \vdots \end{bmatrix}.$$

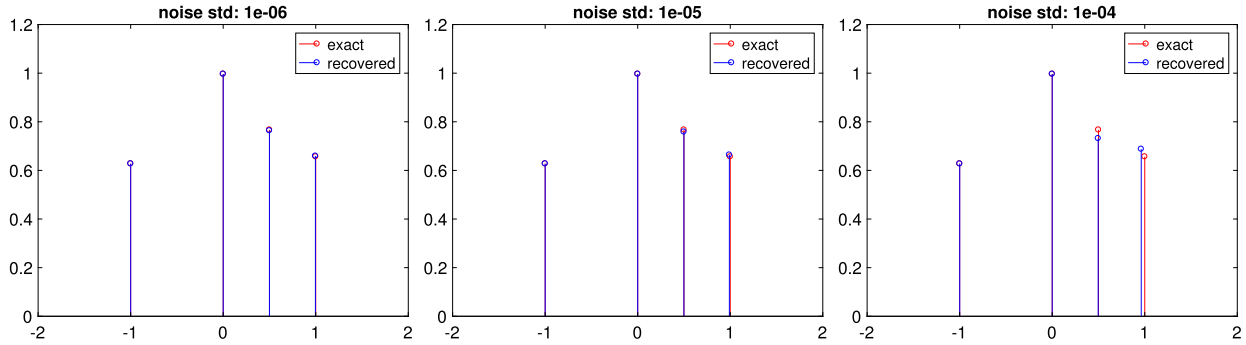

Fig. 5. Sparse support and gapless case. The support of $A(x)$ contains the origin. Results at different noise levels.

For any τ_j

$$S\begin{bmatrix}\tau_j^0\\ \tau_j^1\\ \vdots\end{bmatrix}=\begin{bmatrix}\tau_j^1\\ \tau_j^2\\ \vdots\end{bmatrix},\quad \text{i.e.,}\quad (S-\tau_j)\begin{bmatrix}\tau_j^0\\ \tau_j^1\\ \vdots\end{bmatrix}=0.$$

Since the operators $S-\tau_j$ all commute,

$$\prod_\ell (S-\tau_\ell)\begin{bmatrix}\tau_j^0\\ \tau_j^1\\ \vdots\end{bmatrix}=0. \tag{15}$$

Since $\hat{G}_-$ is a linear combination of such semi-infinite vectors with weights T_j,

$$\prod_\ell (S-\tau_\ell)\hat{G}_-=0.$$

Introduce the polynomial $\prod_\ell (t-\tau_\ell)\equiv p(t)\equiv p_0t^0+\cdots+p_dt^d$, where the degree d is equal to the number of poles inside $\mathbb{D}$. Then (15) becomes

$$p(S)\hat{G}_-\equiv p_0(S^0\hat{G}_-)+\cdots+p_d(S^d\hat{G}_-)=0,\quad \text{i.e.,}\quad \begin{bmatrix}\hat{G}_{-1} & \hat{G}_{-2} & \cdots & \hat{G}_{-(d+1)}\\ \hat{G}_{-2} & \hat{G}_{-3} & \cdots & \hat{G}_{-(d+2)}\\ \vdots & \vdots & \ddots & \vdots\end{bmatrix}\begin{bmatrix}p_0\\ \dots\\ p_d\end{bmatrix}=0. \tag{16}$$

This implies that the number of poles $\{\tau_j\}$ is equal to the smallest value d such that the matrix in (16) is rank deficient. $[p_0,\dots,p_d]^{\mathsf{T}}$ can be computed as a non-zero vector in the null-space of this matrix and the roots of $p(t)=p_0t^0+\ldots+p_dt^d$ are the poles $\{\tau_j\}$ in $\mathbb{D}$.

Step 4. Applying the map (14) to $\{\tau_j\}$ leads to the poles $\{\xi_j\}$, i.e., the support of $A(x)$ in the z plane. With $\{\xi_j\}$ located, we solve the constrained convex optimization problem

$$\min_{A_j\geq 0}\sum_i\left|G(z_i)-\sum_j\frac{A_j}{z_i-\xi_j}\right|^2 \tag{17}$$

for $\{A_j\}$.

Numerical results. The inverse temperature is $\beta=100$ and the number of Matsubara points is $N=128$. The noise in $G(z_n)$ is still additive as in (13). We comment that the gapless case is more difficult, since one can always regard the gapped case as a special instance of the gapless case. Due to the increased difficulty, the noise levels in this experiment are smaller: $\sigma=10^{-6}$, 10^{-5}, and 10^{-4}.

In the first example, the support of the spectral distribution $A(x)$ includes the origin. The numerical results are summarized in Fig. 5. At $\sigma=10^{-6}$, the algorithm gives an accurate reconstruction for both the pole locations and the weights. At $\sigma=10^{-5}$, the reconstruction is still quite accurate. At $\sigma=10^{-4}$, we observe some noticeable errors in the locations and weights.

In the second example, the support of $A(x)$ includes the point 0.01 but not the origin. The numerical results are summarized in Fig. 6. Notice that the reconstruction splits the pole at 0.01 into two poles. Except this issue, the rest of the reconstruction is quite accurate across different noise levels.

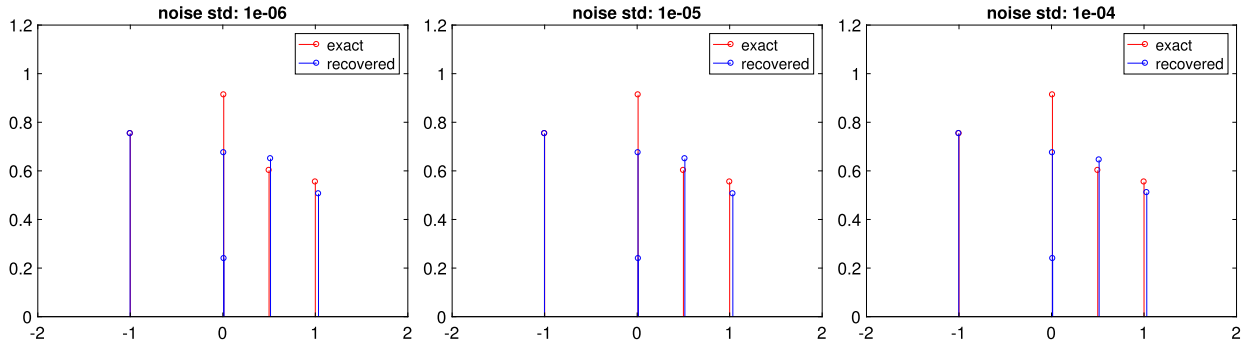

Fig. 6. Sparse support and gapless case. The support of $A(x)$ avoids the origin but contains a nearby point 0.01. Results at different noise levels.

3. Continuous support

In the continuous support case, $A(x) > 0$ on the real axis. The prior is that $G(z)$ can be well-approximated by a small number of pseudo poles in the lower half complex plane, i.e.,

$$G(z) \approx \sum_j \frac{1}{z - \xi_j} A_j$$

where $\{\xi_j\}$ are the poles in the lower half plane and $\{A_j\}$ are the weights.

Step 1. Construct an accurate approximation of $G(z)$ for $z \in [\frac{\pi}{\beta} i, \frac{(2N-1)\pi}{\beta} i]$. To motivate the construction, consider the case of a pole located at $-\eta i$ for $\eta > 0$, i.e., $G(z) \approx \frac{1}{z+\eta i}$. When η is close to zero, $G(z)$ becomes quite steep when z approaches the origin from the positive imaginary axis, making it difficult for standard interpolation and approximation schemes. The key idea is to consider instead $1/G(z) \approx z + \eta i$, which is easy for approximation.

Let us define $H(z) \equiv 1/G(z)$. At the Matsubara points $\{z_n\}$, we have access to $H(z_n) = 1/G(z_n)$. Based on the data $\{(z_n, H(z_n)\}$, construct a high-order spline interpolant $\tilde{H}(z) \approx H(z)$ over the interval $[\frac{\pi}{\beta} i, \frac{(2N-1)\pi}{\beta} i]$. Once this is ready, the function

$$\tilde{G}(z) \equiv 1/\tilde{H}(z) \tag{18}$$

is an accurate approximation to $G(z)$ over $[\frac{\pi}{\beta} i, \frac{(2N-1)\pi}{\beta} i]$ that allows for random access (see Fig. 7(b)).

Step 2. Let $q = \frac{\sqrt{2N-1}\pi}{\beta} i$ and introduce the following sequence of conformal map (from z to w and to t) that unzips the interval $[\frac{\pi}{\beta} i, \frac{(2N-1)\pi}{\beta} i]$ in the z plane to the unit disk $\mathbb{D}$ in the t plane (see Fig. 7(c) and (d))

$$w = \frac{z-q}{z+q}, \quad t = \frac{w}{r} + \sqrt{\frac{w^2}{r^2} - 1}, \tag{19}$$

where $r = \frac{(2N-1)-\sqrt{2N-1}}{(2N-1)+\sqrt{2N-1}}$. The inverse conformal map is

$$z = -q \cdot \frac{w+1}{w-1}, \quad w = \frac{r}{2}\left(t + \frac{1}{t}\right). \tag{20}$$

In the t plane, the push-forward $G(t) \equiv G(z(w(t)))$ of $G(z)$ is analytic outside $\mathbb{D}$ except at the images of $\{\xi_j\}$. Therefore, it takes the form

$$G(t) = \sum_j \frac{T_j}{t - \tau_j} + \text{analytic},$$

where the poles $\{\tau_j\}$ are the images of $\{\xi_j\}$. Again, the key observation is that, if one can identify the poles $\{\tau_j\}$ in the t plane, we can map them back to the z plane to obtain the poles $\{\xi_j\}$ of $G(z)$.

Step 3. Following the discussion in Section 2.1, use Prony's method to identify the poles $\{\tau_j\}$ outside $\mathbb{D}$. This step again involves the Fourier coefficients $\hat{G}_k$ at the positive frequencies.

Step 4. Applying the inverse maps (20) to $\{\tau_j\}$ gives the locations of the pseudo poles $\{\xi_j\}$ in the lower half z plane. With $\{\xi_j\}$ located, solve the constrained convex optimization problem

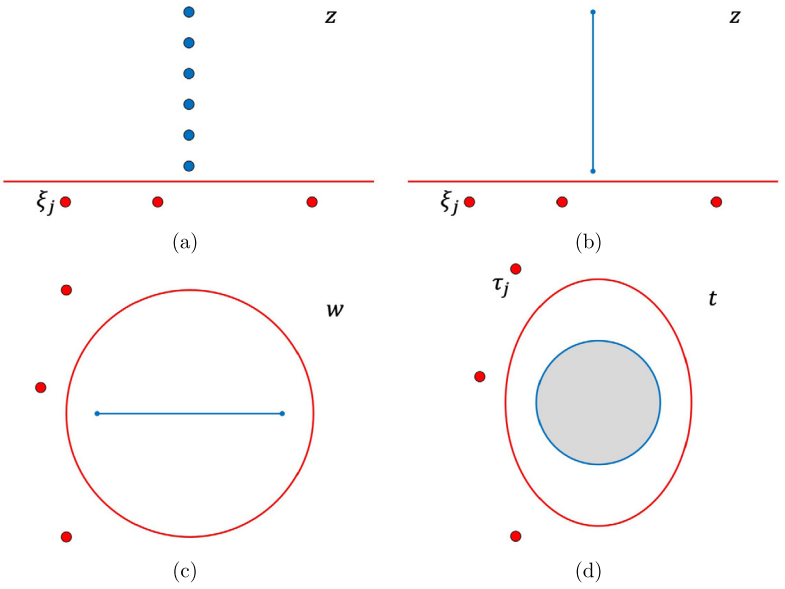

Fig. 7. Continuous support. (a) Problem configuration where the blue dots are the fermionic Matsubara grid and the red dots are the locations of the pseudo poles. (b) $\tilde{G}(z)$ approximation of $G(z)$ over $[\frac{\pi}{\beta}i, \frac{(2N-1)\pi}{\beta}i]$ and allows for random access. (c) The first step of the conformal map brings the real axis to the unit circle and $[\frac{\pi}{\beta}i, \frac{(2N-1)\pi}{\beta}i]$ to a real interval. (d) The second step of the conformal map unzips this real interval into a unit disk. The mapped poles are denoted as $\{\tau_j\}$.

$$\min_{A_j:\forall x\, \mathrm{Im}(\sum_j A_j/(x-\xi_j))\le 0} \sum_i \left| G(z_i) - \sum_j \frac{A_j}{z_i - \xi_j} \right|^2 \tag{21}$$

to compute the weights $\{A_j\}$. Finally, with both $\{\xi_j\}$ and $\{A_j\}$ ready, the spectral function $A(x)$ can be recovered by evaluating

$$-\frac{1}{\pi}\mathrm{Im}\sum_j \frac{A_j}{x + i0^+ - \xi_j}. \tag{22}$$

Notice that the constraint in (21) is included to ensure that (22) is positive.

Implementation details. To implement this algorithm, we need to take care several numerical issues.

- For the spline interpolation for $H(z)$, a fifth order spline is used.
- To compute the Fourier coefficients $\{\hat{G}_k\}$, we again use a uniform grid $\theta_n = \frac{2\pi n}{N_\theta}$ for $n = 0, \ldots, N_\theta - 1$. N_θ is chosen to be a multiple of N to ensure the exponential convergence of the trapezoidal rule.
- The constrained optimization problem (21) is solved with CVX [13].

Numerical results. The inverse temperature is $\beta = 100$ and the number of Matsubara points is $N = 256$. The noise in $G(z_n)$ is again additive as in (13). The noise levels in the experiments are $\sigma = 5 \cdot 10^{-7}, 5 \cdot 10^{-6}, 5 \cdot 10^{-5}$.

In the first example, $A(x)$ corresponds to a sum of pseudo poles at

$$\{-2 - 0.03i, -1 - 0.03i, 0 - 0.03i, 1 - 0.03i, 2 - 0.03i\}$$

and hence the prior used by the algorithm is valid here. The results are summarized in Fig. 8, where we plot $-\frac{1}{\pi}\mathrm{Im}G(x + 0^+i)$ on a horizontal line immediate above the real axis. At $\sigma = 5 \cdot 10^{-7}$, the algorithms give an accurate reconstruction for the spectral function $A(x)$. At $\sigma = 5 \cdot 10^{-6}$, the reconstruction is still quite good, though the magnitude shows some error. At $\sigma = 5 \cdot 10^{-5}$, the reconstructed profile shows some significant error.

In the second example, $A(x)$ is the sum of five Gaussians centered at

$$\{-2, -1, 0, 1, 2\},$$

each with variance equal to $5 \cdot 10^{-3}$. For this example, the prior is misspecified. The results are summarized in Fig. 9. At $\sigma = 5 \cdot 10^{-7}$, the peak locations are well identified but the widths and heights are a bit off. At $\sigma = 5 \cdot 10^{-6}$, there is a shift towards the center for the two Gaussians farthest from the origin. At $\sigma = 5 \cdot 10^{-5}$, the reconstructed profile shows some significant errors.

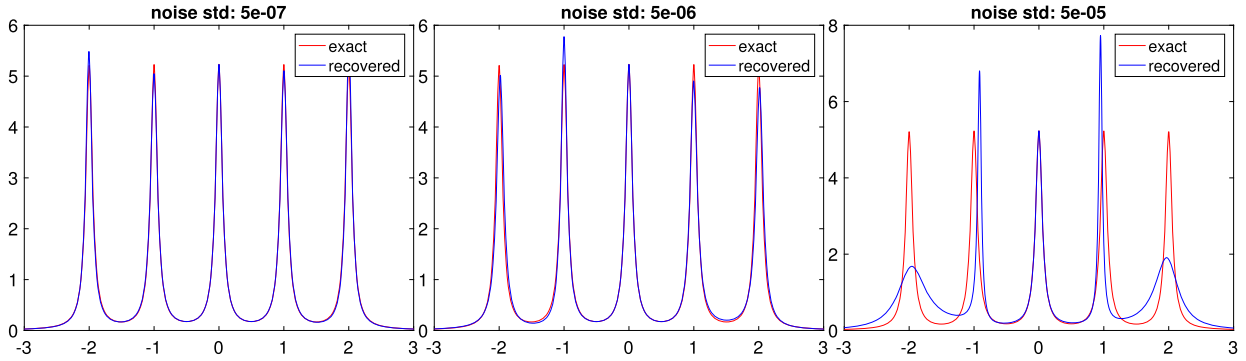

Fig. 8. Continuous support. The spectral function $A(x)$ corresponds to a sum of pseudo poles in the lower half plane. Results at difficult noise levels.

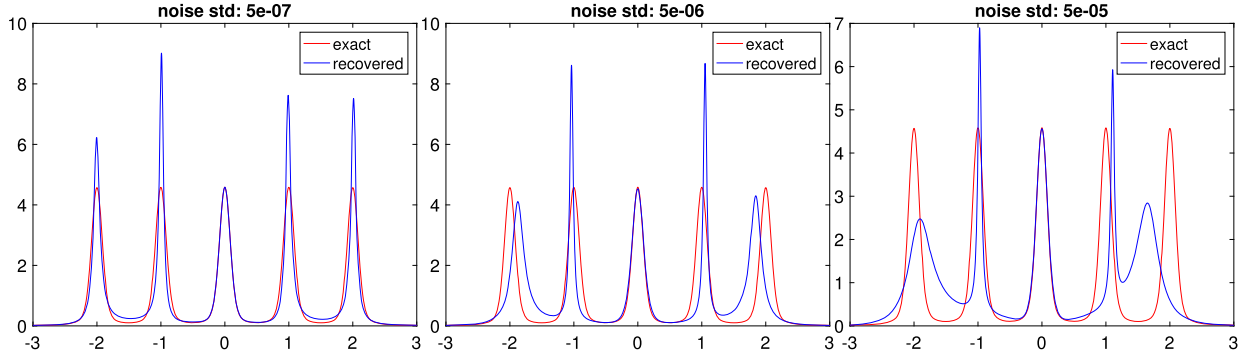

Fig. 9. Continuous support. The spectral function $A(x)$ is equal to a sum of five Gaussians on the real axis. Results at difficult noise levels.

CRediT authorship contribution statement

The author Lexing Ying is responsible for every part of this paper, including designing the method, implementing the code, and writing the paper.

Declaration of competing interest

The authors declare that they have no known competing financial interests or personal relationships that could have appeared to influence the work reported in this paper.

Data availability

No data was used for the research described in the article.

References

[1] K.S.D. Beach, Identifying the maximum entropy method as a special limit of stochastic analytic continuation, arXiv preprint cond-mat (2004).
[2] K.S.D. Beach, R.J. Gooding, F. Marsiglio, Reliable padé analytical continuation method based on a high-accuracy symbolic computation algorithm, Phys. Rev. B 61 (8) (2000) 5147.
[3] Mario Berljafa, Stefan Guttel, The rkfit algorithm for nonlinear rational approximation, SIAM J. Sci. Comput. 39 (5) (2017) A2049–A2071.
[4] Jean-Paul Berrut, Lloyd N. Trefethen, Barycentric lagrange interpolation, SIAM Rev. 46 (3) (2004) 501–517.
[5] Gregory Beylkin, Lucas Monzón, On approximation of functions by exponential sums, Appl. Comput. Harmon. Anal. 19 (1) (2005) 17–48.
[6] Gregory Beylkin, Lucas Monzón, Nonlinear inversion of a band-limited fourier transform, Appl. Comput. Harmon. Anal. 27 (3) (2009) 351–366.
[7] Henrik Bruus, Karsten Flensberg, Many-Body Quantum Theory in Condensed Matter Physics: an Introduction, OUP, Oxford, 2004.
[8] Semyon Dyatlov, Maciej Zworski, Mathematical Theory of Scattering Resonances, Vol. 200, American Mathematical Soc., 2019.
[9] Jiani Fei, Chia-Nan Yeh, Emanuel Gull, Nevanlinna analytical continuation, Phys. Rev. Lett. 126 (5) (2021) 056402.
[10] Jiani Fei, Chia-Nan Yeh, Dominika Zgid, Emanuel Gull, Analytical continuation of matrix-valued functions: Carathéodory formalism, Phys. Rev. B 104 (16) (2021) 165111.
[11] Pedro Gonnet, Stefan Guttel, Lloyd N. Trefethen, Robust padé approximation via svd, SIAM Rev. 55 (1) (2013) 101–117.
[12] Olga Goulko, Andrey S. Mishchenko, Lode Pollet, Nikolay Prokof'ev, Boris Svistunov, Numerical analytic continuation: answers to well-posed questions, Phys. Rev. B 95 (1) (2017) 014102.
[13] Michael Grant, Stephen Boyd, CVX: Matlab Software for Disciplined Convex Programming, Version 2.1, 2014.

[14] Bjorn Gustavsen, Adam Semlyen, Rational approximation of frequency domain responses by vector fitting, IEEE Trans. Power Deliv. 14 (3) (1999) 1052–1061.
[15] Mark Jarrell, James E. Gubernatis, Bayesian inference and the analytic continuation of imaginary-time quantum monte carlo data, Phys. Rep. 269 (3) (1996) 133–195.
[16] Gernot J. Kraberger, Robert Triebl, Manuel Zingl, Markus Aichhorn, Maximum entropy formalism for the analytic continuation of matrix-valued green's functions, Phys. Rev. B 96 (15) (2017) 155128.
[17] Igor Krivenko, Malte Harland, Triqs/som: implementation of the stochastic optimization method for analytic continuation, Comput. Phys. Commun. 239 (2019) 166–183.
[18] Ryan Levy, J.P.F. LeBlanc, Emanuel Gull, Implementation of the maximum entropy method for analytic continuation, Comput. Phys. Commun. 215 (2017) 149–155.
[19] Carlos Mejuto-Zaera, Leonardo Zepeda-Núñez, Michael Lindsey, Norm Tubman, Birgitta Whaley, Lin Lin, Efficient hybridization fitting for dynamical mean-field theory via semi-definite relaxation, Phys. Rev. B 101 (3) (2020) 035143.
[20] Yuji Nakatsukasa, Olivier Sète, Lloyd N. Trefethen, The aaa algorithm for rational approximation, SIAM J. Sci. Comput. 40 (3) (2018) A1494–A1522.
[21] Daniel Potts, Manfred Tasche, Parameter estimation for nonincreasing exponential sums by prony-like methods, Linear Algebra Appl. 439 (4) (2013) 1024–1039.
[22] R. Prony, Essai experimental et analytique, J. Éc. Polytech. (1795) 24–76.
[23] Michael Rumetshofer, Daniel Bauernfeind, Wolfgang von der Linden, Bayesian parametric analytic continuation of green's functions, Phys. Rev. B 100 (7) (2019) 075137.
[24] Anders W. Sandvik, Stochastic method for analytic continuation of quantum monte carlo data, Phys. Rev. B 57 (17) (1998) 10287.
[25] Johan Schött, Inka LM Locht, Elin Lundin, Oscar Grånäs, Olle Eriksson, Igor Di Marco, Analytic continuation by averaging padé approximants, Phys. Rev. B 93 (7) (2016) 075104.
[26] Lloyd N. Trefethen, Quantifying the ill-conditioning of analytic continuation, BIT Numer. Math. 60 (4) (2020) 901–915.
[27] K. Vafayi, O. Gunnarsson, Analytical continuation of spectral data from imaginary time axis to real frequency axis using statistical sampling, Phys. Rev. B 76 (3) (2007) 035115.
[28] H.J. Vidberg, J.W. Serene, Solving the eliashberg equations by means ofn-point padé approximants, J. Low Temp. Phys. 29 (3) (1977) 179–192.
[29] Heather Wilber, Anil Damle, Alex Townsend, Data-driven algorithms for signal processing with rational functions, arXiv preprint arXiv:2105.07324, 2021.
[30] Lexing Ying, Pole recovery from noisy data on imaginary axis, arXiv preprint arXiv:2202.02670, 2022.